Turbulent boundary layer response to the introduction of stable stratification

T. Van Buren[1], O. Williams[1] and A. J. Smits[1,2]

May 17, 2019

Abstract

The response of an initially neutral rough-wall turbulent boundary layer to a change in wall temperature is investigated experimentally. The change causes a localized peak in stable stratification that diffuses and moves away from the wall with downstream distance. The streamwise and wall-normal components of turbulent velocity fluctuations are damped at similar rates, even though the stratification only directly impacts the wall-normal component. The Reynolds shear profiles reveal the growth of an internal layer that scales approximately with the bulk Brunt-Väisälä frequency.

1 Introduction

Buoyancy forces have a stabilizing effect on boundary layers when they act in the direction towards the wall. Such thermally stable flows are found in nocturnal atmospheric boundary layers where the air is warmer than the ground, and winds in the polar region where warm air flows over cold seas or ice. They may also be encountered in industrial settings such as plate heat exchangers. Stable stratification reduces turbulent mixing by inhibiting vertical transport, thereby significantly reducing heat and momentum transfer across the layer. With strong stable stratification the turbulent structure changes significantly, and additional flow features such as large-scale intermittency, gravity waves and Kelvin-Helmholtz instabilities become more important, invalidating many conventional boundary layer concepts (Mahrt, 1998, 1999).

A number of experimental studies have examined the behavior of thermally stable boundary layers (Arya, 1975; Ogawa *et al.*, 1985; Ohya *et al.*, 1997; Ohya, 2001). These investigations indicate a progressive dampening of turbulence with increasing stratification characterized by the bulk Richardson number,

$$Ri_\delta = \frac{g\delta}{U_\infty^2}\frac{\Delta T}{T_\infty}, \tag{1}$$

where g is the acceleration due to gravity, δ is the boundary layer thickness, ΔT is the temperature difference across the layer, and T_∞ and U_∞ are the

freestream temperature and velocity, respectively. For stable boundary layers, the Richardson number is positive.

More recently, Williams *et al.* (2016) reported a parametric study of stably stratified boundary layers for momentum thickness Reynolds numbers of $600 \leq Re_\theta \leq 2400$ and bulk Richardson numbers up to $Ri_\delta \approx 0.25$. Here, $Re_\theta = U_\infty \theta / \nu_\infty$, ν_∞ is the fluid kinematic viscosity at the freestream temperature, and the momentum thickness θ is defined according to

$$\theta = \int_0^\infty \frac{\rho U}{\rho_\infty U_\infty} \left(1 - \frac{U}{U_\infty}\right) dz \tag{2}$$

(U and ρ are the streamwise velocity and fluid density, respectively). It was found that for weak to moderate stability, the turbulent stress profiles scaled with the density weighted friction velocity u_*, while the mean velocity profiles changed to a more laminar shape. Here, $u_* = \sqrt{\rho/\rho_w} u_\tau$, where $u_\tau = \sqrt{\tau_w/\rho_w}$, τ_w is the wall stress, and ρ_w is the fluid density at the wall. The success in scaling the turbulent stresses with u_* suggests little change in turbulent structure for moderate levels of stability. As in previous studies, the turbulent production was observed to collapse at higher Richardson numbers, resulting in patchy and highly intermittent turbulence.

Here, we are interested in the response of an initially neutral turbulent boundary layer to a change in wall temperature, leading to the progressive development of stable stratification. This type of flow is encountered, for example, in daytime summer offshore breezes where warm air flows from land onto a cooler ocean, and in the flow over ice packs in the arctic. By studying such flows we hope to improve our understanding of these atmospheric processes.

In a more general context, the response of wall-bounded flows to perturbations in wall boundary conditions have been examined reasonably extensively (Smits & Wood, 1985; Garratt, 1990), and examples include sudden changes in surface roughness (Wood, 1982; Antonia & Luxton, 1971, 1972; Taylor *et al.*, 1987), blowing/suction (Simpson, 1971; Squire *et al.*, 1977), wall heat flux (Antonia *et al.*, 1977; Fedorovich *et al.*, 1996), and wall temperature (Johnson, 1957; Ligrani & Moffat, 1985; Mukerji *et al.*, 2004). The latter four studies are perhaps most closely related to the present work, but in all cases the perturbations were "weak" in that local similarity was preserved. Such weak step changes are commonly described in terms of the growth of an internal layer where the flow scales with the local wall shear, and an overlying external layer that continues to scale with the conditions upstream of the step. The extent of the internal layer is often seen to grow at a rate typical of a turbulent boundary layer, that is $\delta_i \sim \bar{x}^{0.8}$, where $\bar{x} = x - x_0$ is the distance downstream of the step, x is the distance measured from the origin of the boundary layer and x_0 is the distance from the boundary layer origin to the step. When $\bar{x}$ exceeds 10 to 20δ, the internal layer has usually grown to the full extent of the boundary layer, although the relaxation distance for the turbulence is often much longer than that for the mean flow (Alving *et al.*, 1990).

In terms of more severe step changes in wall temperature, Hara *et al.* (2009) examined a destabilizing case, transitioning from a cooled to a heated floor.

Also, Mahrt (2000) presented scaling arguments for the influence of surface heterogeneity of different types and sizes, and Stoll & Porté-Agel (2009) performed large-eddy simulations of stably stratified atmospheric boundary layers over a surface with temperature transition patches. In these simulations, the effects of small patches (0.5 to 2δ long) with a variety of temperature differences were studied in the very near field of the step change ($\bar{x} < 4\delta$), and the turbulent stresses were either amplified or damped within the internal layer, depending on whether the step change was destabilizing or stabilizing.

Here, we complement these simulations with an experimental study on the effects of imposing stable stratification on an initially neutral turbulent boundary layer. The surface is rough everywhere, and at the point where the flow encounters the change in wall temperature $Re_\theta = 1280$. The wall temperature differences produced Richardson numbers as high as $Ri_\delta = 0.2$. We find that the buoyancy time scale, that is, the inverse of the (bulk) Brunt-Väisälä frequency $N = \sqrt{(g/\delta)\Delta T/T_\infty}$, is an important parameter to describe the response of the turbulent stresses, and the rate of growth of the internal layer (N may be interpreted as the frequency of oscillation of a fluid particle whose position is perturbed in the presence of a density gradient).

2 Experimental Setup

The boundary layer developed on the upper wall of a wind tunnel, as shown in figure 1. The wind tunnel is a suction type with a $1.2 \times 0.9 \times 5$ m test section, operated at a fixed freestream velocity of $U_\infty = 1.5$ m/s. The boundary layer was tripped using a 6.35 mm rod at the test section inlet and maintained with a square-weave wire mesh surface roughness having a wire mesh thickness of $k = 4.1$ mm, which corresponds to $k^+ = ku_\tau/\nu_w \approx 24$, and an equivalent sand grain roughness of $k_s^+ = 49$, as defined by Nikuradse (1933), where

$$\Delta U^+ = \frac{1}{\kappa} ln(k_s^+) + B - 8.5. \tag{3}$$

Here, κ and B are the slope and intercept of the logarithmic portion of the mean velocity profile; and the superscript + denotes scaling using the friction velocity u_τ and inner length scale ν_w/u_τ. The ratio of the boundary layer height to roughness height is $\delta/k = 26$. The boundary layer height at the beginning of our measurement region is δ_0=10.7 cm, which is defined as the wall-normal location at which the local mean velocity peaks (the profiles displayed a small overshoot near the edge of the layer). All values correspond to the conditions at $x = 2.44$ m for the neutral boundary layer (isothermal wall).

For $x \geq 2.44$ m ($\bar{x} \geq 0$), the aluminum ceiling of the test section was heated using strip heating elements to generate the change in wall temperature. Because of the orientation of the wall, this heating leads to stable stratification. The boundary layer at the start of the heating had a height of $\delta_0 = 0.105$ m and $Re_\theta = 1280$. The wall temperature for $x > x_0$ was varied from $0 \leq \Delta T \leq 120$ K, where $\Delta T = T_w - T_\infty$ (wall and freestream values denoted with

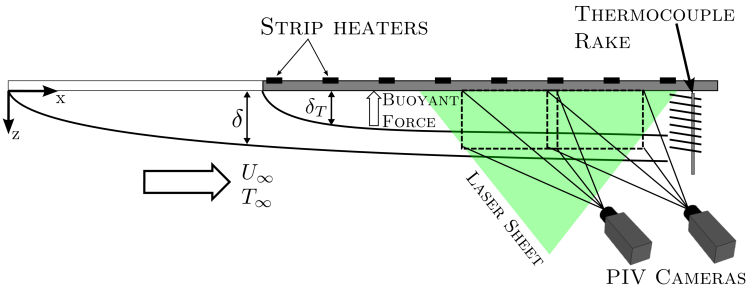

Figure 1: Schematic of the experimental setup.

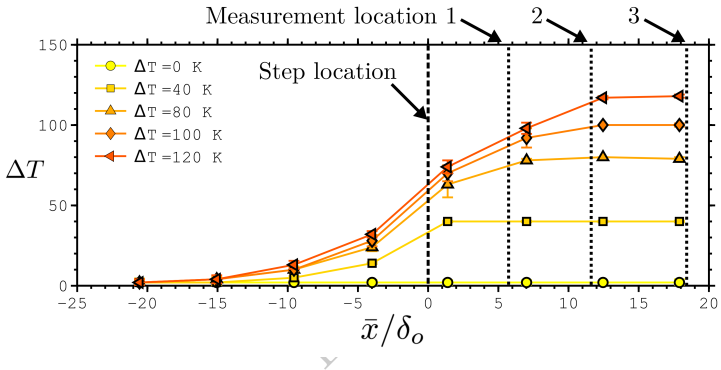

Figure 2: Wall temperature as it varies downstream for different wall temperatures. Temperature introduction and measurement locations are as marked.

subscripts w and ∞, respectively). The wall temperatures were monitored using multiple thermocouples installed on the test surface centerline, and the variation of temperature with downstream distance is shown in figure 2 for each of the test conditions. The uncertainty bars denote the standard deviation of the wall temperature at that location for over the entire experiment. We see that the change in temperature occurs over a distance of about 10 to $15\delta_0$ due to longitudinal heat conduction in the aluminum wall. Thus, at each measurement location we have the nominal and actual wall temperature differences, ΔT and ΔT_a respectively.

All test conditions are given in table 1. Here, $C_f = 2\tau_w/(\rho_\infty U_\infty^2)$, δ is the local boundary layer thickness, and $Re_\tau = \delta u_\tau/\nu_w$. At the furthest downstream station the bulk Richardson number Ri_δ reaches a maximum value of 0.2.

We use two reference cases to describe the state of flow in the absence of the change in wall temperature. The first reference case is the state of the flow at the first measurement location with no heating ($\Delta T = 0$), referred to as the

$\bar{x}/\delta_o$	ΔT $[K]$	ΔT_a $[K]$	δ $[mm]$	Re_θ	Re_τ	Ri_δ	$C_f \times 10^3$	k^+	symbol
5.7	0	0	105	1277	629	0	7.06	24.4	▲
	40	39	104	1228	487	0.06	6.08	19.3	
	80	65	104	1211	419	0.10	5.44	16.6	
	100	63	104	1172	430	0.09	5.77	16.9	
	120	77	102	1142	386	0.11	5.36	15.7	
11.6	0	0	116	1478	690	0	6.85	24.2	●
	40	43	116	1419	513	0.07	5.32	18.2	
	80	81	116	1356	399	0.13	4.25	14,2	
	100	88	116	1366	375	0.15	3.92	13.3	
	120	98	114	1297	370	0.16	4.18	13.2	
18.2	0	0	125	1628	802	0	7.50	26.0	■
	40	42	124	1502	574	0.07	5.68	19.2	
	80	80	124	1444	451	0.14	4.60	15.2	
	100	101	124	1398	388	0.17	3.88	13.1	
	120	117	124	1379	353	0.20	3.61	11.8	

Table 1: Test conditions at each downstream location.

neutral case. The second reference case is the state of the flow with heating applied along the entire length of the test section, referred to as the developed stabilization case. The reference cases are taken from Williams (2014) and Williams *et al.* (2016) who performed experiments using the same apparatus. Note that each wall temperature has a corresponding developed stabilization case.

Planar particle image velocimetry (PIV) measurements were taken at three downstream locations, $\bar{x}/\delta_0 = 5.7$, 11.6, and 18.2 (marked in figure 2). A large field-of-view (window size $2.86\,\delta_0 \times 1.5\,\delta_0$) was achieved by using two overlapping PIV windows that were stitched together during processing. The LaVision PIV system used two 5.5 mega-pixel sCMOS cameras and a dual-pulsed 50 mJ Nd:YAG laser. Mineral oil smoke particles from a MAX 3000 MDG fog generator of approximately 1 μm in diameter were used for flow seeding. Further details on the PIV system and data processing techniques are given in Williams (2014) and Williams *et al.* (2016). The random error of the PIV velocity measurements was estimated to be less than 1% of the freestream velocity.

In the higher wall temperature cases the seeding of the flow field near the wall was more sparse as the seeding particles tended to evaporate. Hence, a wall-normal height is defined ($z_{10\%}$) which is the location below which more than 10% of the vectors were removed from the post-processing due to having a peak ratio less than 1.1, in conjunction with a normalized median filter (Westerweel & Scarano, 2005) greater than two standard deviations of a 5×5 neighborhood. Below this height, the results are shown without symbols in the plots.

Temperature profiles were measured using a thermocouple rake. The rake spanned a wall-normal distance of 128.6 mm, with a thermocouple spacing that

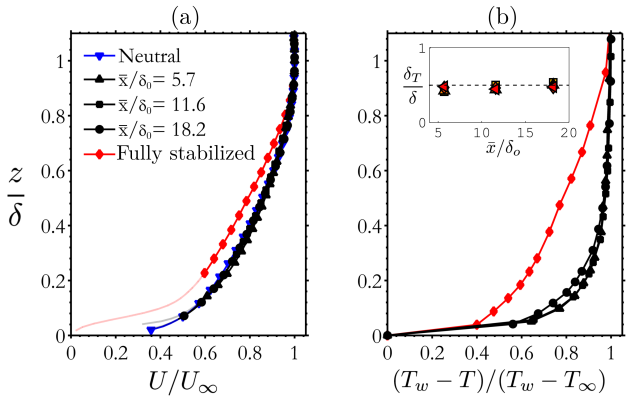

Figure 3: (a) Mean velocity profiles, and (b) temperature profiles for $\Delta T = 120$K. The inset shows the ratio of the thermal boundary layer thickness δ_T to the velocity boundary layer thickness δ at the same location for each wall temperature (symbols for inset as in figure 2).

varied from a minimum of 4.8 mm near the wall, increasing to a maximum of 19 mm near the freestream. Calibrated macro photography was used to determine the wall-normal distance of the first thermocouple. All thermocouples were monitored using a National Instruments PCI-6229 board through LabView, accurate to $\pm 1°$C.

3 Results

The mean velocity and temperature profiles are shown in figure 3. Whereas the mean velocity is almost unaffected by the change in wall temperature, the temperature layer is established very quickly, occupying about 50% of the velocity boundary layer by the first measurement station ($\bar{x}/\delta_0 = 5.7$). Further downstream the temperature layer grows very slowly, with some filling out of the profile evident at the most downstream measurement location for $\Delta T = 120$K. To find the skin friction coefficient C_f, the wall stress τ_w was approximated using the peak in the total stress distribution. The results, shown in figure 4, indicate that the skin friction is slow to respond to the change in buoyancy, but then gradually decreases further downstream by an amount that grows with increasing degree of stratification. Changing the reference density in the skin friction coefficient from ρ_∞ to ρ_w did little to change this trend.

The gradient Richardson number is a local estimate of the stratification effect (as opposed to the bulk Richardson number which is a mean value across the layer), and is defined according to

$$Ri = \frac{g}{T_\infty} \frac{\partial T/\partial z}{(\partial U/\partial z)^2}. \tag{4}$$

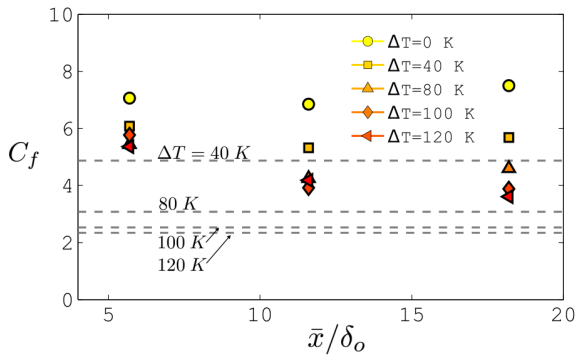

Figure 4: Skin friction coefficient variation. Dashed lines represent the skin friction coefficient for the developed stabilization cases.

Figure 5 shows the gradient Richardson number profiles. The temperature and velocity gradients were computed as in Williams *et al.* (2016). The data for $z/\delta_0 \geq 0.75$) is indicated using a faint line because the gradients in this region become very small, and the accuracy of the data is questionable. We see that the trends are consistent across all levels of stratification. Near the wall, the gradient Richardson number increases almost linearly with wall-normal distance, with the extent of this linear variation increasing with increasing bulk stability and downstream distance. Beyond this region, a local peak in the gradient Richardson number develops, which is especially evident at the furthest downstream location. The peak is due to the temperature field reacting to the wall-temperature change faster than the velocity field (see figure 3). The local gradient Richardson number exceeds the developed case near the wall for the strongest levels of stratification, indicating some non-equilibrium effects.

The stratification has a strong and immediate impact on the turbulence, as seen in figure 6. Here, $\overline{u^2}$ is the variance of the streamwise velocity component and $\overline{w^2}$ is the variance of the wall-normal velocity omponent, and we have normalized the data using $u_{\tau 0}$, the friction velocity for the neutral case at $x = x_0$. Williams *et al.* (2016) found that for weak stratification the turbulence profiles scaled with the density weighted friction velocity u_*. As suggested by our observations on the skin friction coefficient, this scaling would not be successful here, again indicating departures from equilibrium. The magnitude of the damping increases with the strength of the stratification, and even the smallest temperature difference produces noticeable changes in the stress profiles close to the location where the wall temperature changes, which was not seen in the mean velocity profiles. For $\Delta T \geq 80$ K, the impact of the change is evident over more than 60% of the boundary layer for the streamwise and the wall-normal components.

To make a more quantitative comparison between the development of the two

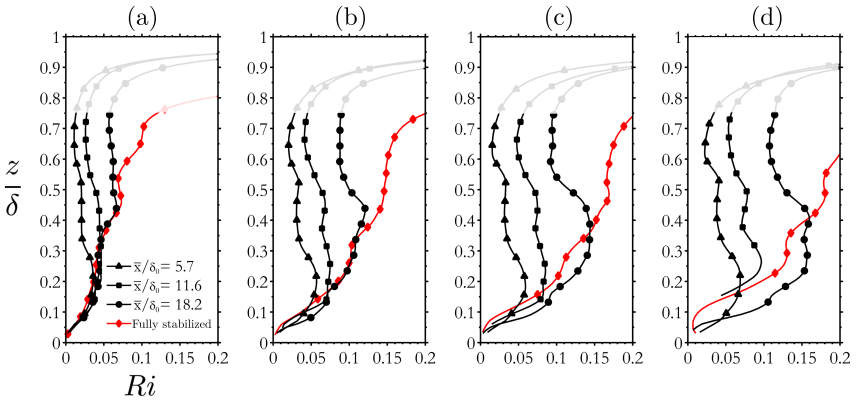

Figure 5: Gradient Richardson number profiles. (a) ΔT =40 K; (b) 80 K, (c) 100 K, (d) 120 K. Data for $z/\delta_0 \geq 0.75$ must be treated with caution due the small magnitudes of the mean gradients.

velocity components, we use the integral parameter λ, defined for the streamwise component by

$$\lambda_u = \frac{\int(\overline{u^2} - \overline{u^2}_{devstab})dz}{\int(\overline{u^2}_{neutral} - \overline{u^2}_{devstab})dz}, \tag{5}$$

with a similar definition of λ_w for the wall-normal component. This parameter represents a bulk measure of the turbulence development, where $\lambda = 0$ for the neutral case, and $\lambda = 1$ when the turbulence matches the developed stabilization case.

From figure 7 we see that λ grows approximately linearly with downstream distance, for this measurement domain and resolution, and the different levels of stability all display similar values. The first implication is that the bulk development is relatively unaffected by the magnitude of the change in wall temperature, and so for all cases the flow will reach the developed stabilization condition at a similar rate. The second implication is that the streamwise and wall-normal components of the velocity are developing at approximately the same rate. This is somewhat surprising because the buoyancy is expected to have a more direct impact on the wall-normal velocity fluctuations.

To help interpret these trends, consider the transport equations for the streamwise and wall-normal components of the turbulence kinetic energy, and for the Reynolds shear stress $-\overline{uw}$. We will neglect streamwise gradients of mean properties on the grounds that the flow evolves rather slowly (so that the usual boundary layer approximations continue to hold), and we will assume that departures from the Boussinesq approximation are not dynamically important. In the outer part of the boundary layer the transport terms are then small, and

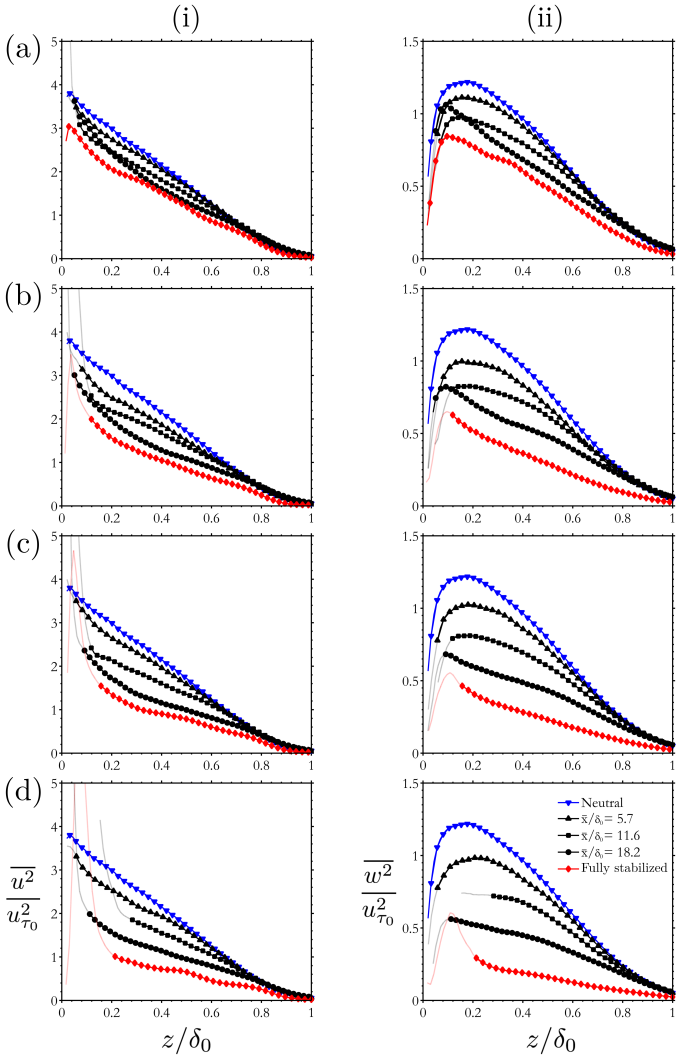

Figure 6: Turbulence intensities normalized using the friction velocity for the neutral case. Left: streamwise component. Right: wall-normal component. (a) ΔT =40 K; (b) 80 K, (c) 100 K, (d) 120 K.

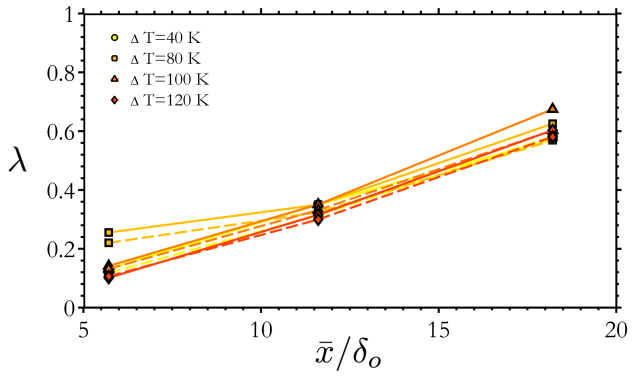

Figure 7: Bulk development parameter for the streamwise (————-) and wall-normal (– – –) components.

so for the streamwise component we have

$$\frac{D\overline{u^2}}{Dt} = -2\overline{uw}\frac{\partial U}{\partial z} + \frac{2}{\rho}\overline{p'\frac{\partial u}{\partial x}} - \epsilon_u. \tag{6}$$

where p' is the pressure fluctuation, and ϵ_u is the streamwise velocity dissipation term. Similarly, we have for the wall-normal component (note that in our case gravity acts in the direction opposite to the direction of the temperature increase),

$$\frac{D\overline{w^2}}{Dt} = \frac{2}{\rho}\overline{p'\frac{\partial w}{\partial z}} + 2\frac{g}{T_0}\overline{wT'} - \epsilon_w \tag{7}$$

where T' is the temperature fluctuation and ϵ_w is the wall-normal velocity dissipation term. For the Reynolds shear stress, only the production and the pressure strain terms are important in the outer layer, so

$$\frac{D(-\overline{uw})}{Dt} = \overline{w^2}\frac{\partial U}{dz} + \frac{1}{\rho}\left(\overline{p'\frac{\partial u}{\partial z}} + \overline{p'\frac{\partial w}{\partial x}}\right) + \frac{g}{T_0}\overline{uT'}. \tag{8}$$

We see that the wall-normal component loses energy through buoyancy-induced damping ($\overline{wT'} < 0$). In turn, the reduction in $\overline{w^2}$ tends to reduce the production of $-\overline{uw}$, with a further reduction through buoyancy ($\overline{uT'} < 0$). Next, the streamwise component is reduced by a decrease in (positive) production. Hence, the buoyancy directly extracts energy from the wall-normal turbulence, but the streamwise turbulence is impacted mostly by the change in Reynolds shear stress. See also the related findings of Arya (1975) and Shah & Bou-Zeid (2014). We note from figure 7 that the wall-normal component lags the streamwise component by a distance $O(\delta)$, which is typical of a large eddy turnover time, and so this exchange among the components of the Reynolds

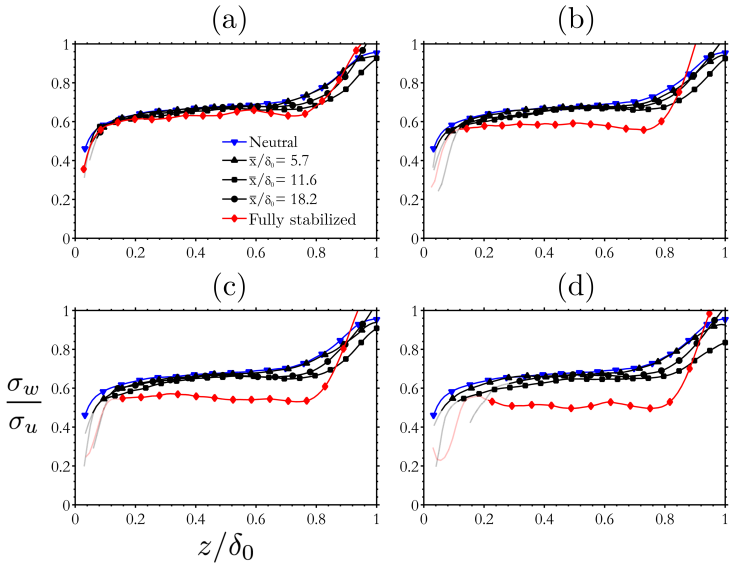

Figure 8: Anisotropy ratio profiles. (a) ΔT =40 K; (b) 80 K, (c) 100 K, (d) 120 K.

stress through the pressure-strain term and buoyancy-driven damping occurs over a similar distance.

To explore this coupling further, we show the anisotropy ratio σ_w/σ_u in figure 8, where $\sigma_u = \sqrt{\overline{u^2}}$ and similarly for σ_w. The anisotropy ratio is almost constant across the boundary layer, and it demonstrates a very slow tendency toward the developed stabilization cases (especially for the higher temperature differences). Arya (1975) and Williams *et al.* (2016) also noted that the anisotropy ratio for equilibrium boundary layers is relatively insensitive for weak to moderate levels of stability.

The Reynolds shear stress profiles are given in figure 9. As seen in the streamwise and wall-normal stresses, stability reduces the Reynolds shear stress, and the effects grow with downstream distance. On figure 9d, ζ denotes the wall-normal distance where the profiles match the neutral case. This point is taken to be a measure of the wall-normal extent of the impact of the change in wall temperature. The variation of ζ with downstream distance is shown in figure 10. The uncertainty bars are associated with the error in the estimate of ζ which was determined from the standard deviation between five separate visual estimates. The results were found to collapse within the measurement domain when the streamwise distance $\bar{x}$ is normalized by a distance given by U_∞/N, where N is the (bulk) Brunt-Väisälä frequency, so that we have a non-dimensional parameter

$$\frac{\bar{x}N}{U_\infty} = \sqrt{\frac{\bar{x}^2}{\delta}\frac{g}{U_\infty^2}\frac{\Delta T}{T_\infty}} = \frac{\bar{x}}{\delta}\sqrt{Ri_\delta}. \tag{9}$$

The variation of ζ can be fitted by a power law function $(\bar{x}N/U_\infty)^n$, where n varies from about 0.15 to 0.35 for the range of virtual origins encompassed by the beginning and the end of the wall temperature rise. A smaller exponent will make the growth steeper for small values of x, and less steep for large values, and so this internal layer grows more quickly close to the step and then more slowly downstream when compared to a typical growth rate of $x^{0.8}$ for an internal layer produced by a weak perturbation.

Our observation that the extent of the internal layer increases with the level of stable stratification is somewhat surprising. At first sight, we expect the opposite trend, in that thermal stability leads to decreased mixing (see Garratt 1990 for discussion on internal boundary layer growth and Chung & Matheou 2012 for a summary of this scaling in unbounded homogeneous stratified shear turbulence). Our data more closely follows the model of Venkatram (1977) for step changes in surface temperature or moisture which is most often applied to unstable and approximately neutrally stratified flows and suggests that the internal layer growth increases with the strength of the disturbance. However, Williams *et al.* (2016) observed that decreases in mixing for weak to moderate levels of stability were proportional to reductions in the wall-shear stress and continued to follow the scaling laws for neutrally stratified flows (when accounting for changes in fluid density). The results from the present study appears to fall in the same weak to moderate stability regime, as indicated by the insensitivity of the anisotropy parameter to the change in wall temperature. It seems plausible, therefore, that the growth of internal layer observed here more closely follows trends seen in neutrally stratified flows since the mixing processes seem to be largely unchanged by the presence of stability. It should also be noted that our scaling is based on an outer layer measurement, whereas atmospheric measurements are limited to the inner layer.

4 Conclusions

A thermally stable stratified boundary layer subject to a change in wall temperature was examined for a range of temperatures. The mean velocity profile showed little change over the range of streamwise location studied, but the temperature layer was established quickly but then showed little evolution downstream. This evolution was reflected in the local gradient Richardson number distributions, with localized peaks appearing in the profile that moved away from the wall and diffused downstream. This peak is likely due to the fast evolution of the mean temperature profile relative to the velocity profile.

The streamwise and wall-normal components of the turbulent stress were damped at approximately equal rates by the effects of buoyancy, indicating a strong coupling between the wall-normal and streamwise components on a time

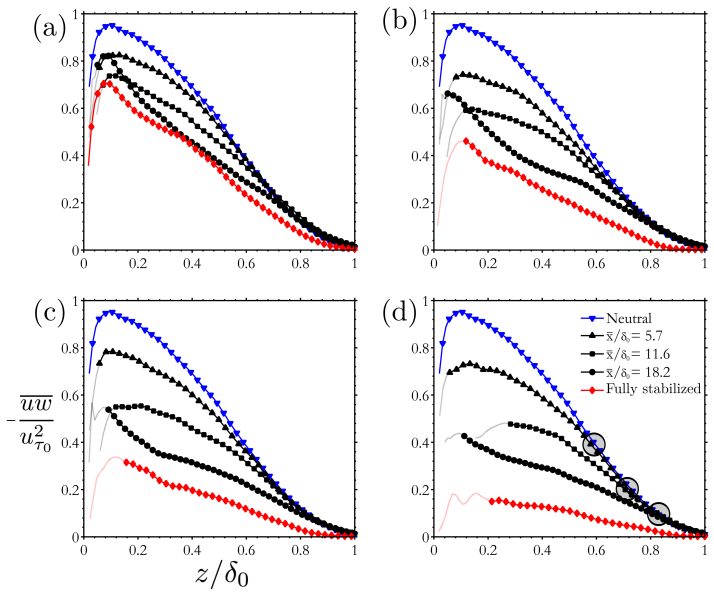

Figure 9: Reynolds shear stress profiles. (a) ΔT =40 K; (b) 80 K, (c) 100 K, (d) 120 K. Circles on (d) mark the wall-normal extent where the boundary layer scales with the upstream boundary condition.

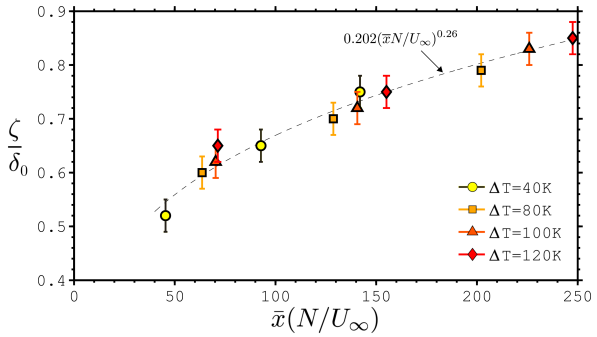

Figure 10: Wall-normal extent of the impact of the change in stable stratification on the Reynolds shear stress.

scale typical of a large eddy turnover time ($O(\delta/U_\infty)$). The local response, as measured by bulk development parameters, grew linearly downstream at about the same rate for both components, invariant of the level of stability, suggesting that the rate of response was largely independent of the magnitude of the step change. The Reynolds shear stress was used to identify the internal layer, and the growth of this inner layer approximately followed a $(\bar{x}N/U_\infty)^{0.26}$ power law where N is the bulk Brunt-Väisälä frequency. Hence, it appears that the local turbulence response is on a scale of the eddy turnover time, and the asymptotic response is governed by the Brunt-Väisälä frequency. The ratio of these time scales is simply given by $N\delta/U_\infty$, known as the inverse Froude number, that is, $\sqrt{Ri_\delta}$.

This work was supported in part by the Cooperative Institute for Climate Science (CICS) at Princeton University.

References

Alving, Amy E, Smits, Alexander J & Watmuff, Jonathan H 1990 Turbulent boundary layer relaxation from convex curvature. *Journal of Fluid Mechanics* **211**, 529–556.

Antonia, R.A., Danh, H.Q. & Prabhu, A. 1977 Response of a turbulent boundary layer to a step change in surface heat flux. *Journal of Fluid Mechanics* **80** (01), 153–177.

Antonia, R.A. & Luxton, R.E. 1971 The response of a turbulent boundary layer to a step change in surface roughness part 1. smooth to rough. *Journal of Fluid Mechanics* **48** (04), 721–761.

Antonia, R.A. & Luxton, R.E. 1972 The response of a turbulent boundary layer to a step change in surface roughness. part 2. rough-to-smooth. *Journal of Fluid Mechanics* **53** (04), 737–757.

Arya, SPS 1975 Buoyancy effects in a horizontal flat-plate boundary layer. *Journal of Fluid Mechanics* **68** (02), 321–343.

Chung, D. & Matheou, G. 2012 Direct numerical simulation of stationary homogenous stratified sheared turbulence. *Journal of Fluid Mechanics* **696**, 434–467.

Fedorovich, E., Kaiser, R., Rau, M. & Plate, E. 1996 Wind tunnel study of turbulent flow structure in the convective boundary layer capped by a temperature inversion. *Journal of the atmospheric sciences* **53** (9), 1273–1289.

Garratt, JR 1990 The internal boundary layera review. *Boundary-Layer Meteorology* **50** (1-4), 171–203.

Hara, Tomohiro, Ohya, Yuji, Uchida, Takanori & Ohba, Ryohji 2009 Wind-tunnel and numerical simulations of the coastal thermal internal boundary layer. *Boundary-layer Meteorology* **130** (3), 365–381.

Johnson, D.S. 1957 Velocity, temperature and heat transfer measurements in a turbulent boundary layer downstream of a stepwise discontinuity in wall temperature. *J. Appl. Mech* **24** (2).

Ligrani, P.M. & Moffat, R.J. 1985 Thermal boundary layers on a rough surface downstream of steps in wall temperature. *Boundary-Layer Meteorology* **31** (2), 127–147.

Mahrt, L. 1998 Stratified atmospheric boundary layers and breakdown of models. *Theoretical and computational fluid dynamics* **11** (3-4), 263–279.

Mahrt, L. 1999 Stratified atmospheric boundary layers. *Boundary-Layer Meteorology* **90** (3), 375–396.

Mahrt, L 2000 Surface heterogeneity and vertical structure of the boundary layer. *Boundary-Layer Meteorology* **96** (1-2), 33–62.

Mukerji, Debjit, Eaton, John K & Moffat, Robert J 2004 Convective heat transfer near one-dimensional and two-dimensional wall temperature steps. *Journal of heat transfer* **126** (2), 202–210.

Nikuradse, J. 1933 Laws of flow in rough pipes. In *VDI Forschungsheft*. Citeseer.

Ogawa, Y, Diosey, PG, Uehara, K & Ueda, H 1985 Wind tunnel observation of flow and diffusion under stable stratification. *Atmospheric Environment (1967)* **19** (1), 65–74.

Ohya, Yuji 2001 Wind-tunnel study of atmospheric stable boundary layers over a rough surface. *Boundary-layer meteorology* **98** (1), 57–82.

Ohya, Yuji, Neff, David E & Meroney, Robert N 1997 Turbulence structure in a stratified boundary layer under stable conditions. *Boundary-Layer Meteorology* **83** (1), 139–162.

Shah, S.K. & Bou-Zeid, E. 2014 Direct numerical simulations of turbulent ekman layers with increasing static stability: modifications to the bulk structure and second-order statistics. *Journal of Fluid Mechanics* **760**, 494–539.

Simpson, R. L. 1971 The effect of a discontinuity in wall blowing on the turbulent incompressible boundary layer. *International Journal of Heat and Mass Transfer* **14** (12), 2083–2097.

Smits, AJ & Wood, DH 1985 The response of turbulent boundary layers to sudden perturbations. *Annual Review of Fluid Mechanics* **17** (1), 321–358.

Squire, L.C., Thomas, G.D. & Marriott, P.G. 1977 Compressible turbulent boundary layers with injection. *AIAA Journal* **15** (3), 425–427.

Stoll, R. & Porté-Agel, F. 2009 Surface heterogeneity effects on regional-scale fluxes in stable boundary layers: surface temperature transitions. *Journal of the Atmospheric Sciences* **66** (2), 412–431.

Taylor, P.A., Mason, P.J. & Bradley, E.F. 1987 Boundary-layer flow over low hills. *Boundary-layer meteorology* **39** (1-2), 107–132.

Venkatram, A 1977 A model of internal boundary-layer development. *Boundary-Layer Meteorology* **11** (4), 419–437.

Westerweel, J. & Scarano, F. 2005 Universal outlier detection for piv data. *Experiments in Fluids* **39** (6), 1096–1100.

Williams, O. 2014 Density effects on turbulent boundary layer structure: from the atmosphere to hypersonic flow. PhD thesis, Princeton University.

Williams, O., Hohman, T., Van Buren, T. & Smits, A. 2016 The effect of stable thermal stratification on turbulent boundary layer statistics. *Journal of Fluid Mechanics* Under Review.

Wood, D.H. 1982 Internal boundary layer growth following a step change in surface roughness. *Boundary-Layer Meteorology* **22** (2), 241–244.